Quantitative absorption imaging: The role of incoherent multiple scattering in the saturating regime

Romain Veyron ⬤, Vincent Mancois ⬤, Jean-Baptiste Gerent ⬤, Guillaume Baclet, Philippe Bouyer ⬤, and Simon Bernon ⬤*

LP2N, Laboratoire Photonique, Numérique et Nanosciences, Université de Bordeaux-IOGS-CNRS:UMR 5298, 1 rue François Mitterrand, F-33400 Talence, France

In this paper, we study the modification of coherent scattering processes in dense ensembles. Using absorption imaging, we experimentally demonstrate that the absorption cross section in dense ^{87}Rb cold atom ensembles is reduced, with respect to the single-particle response. This reduction is linearly dependent on the optical density and well reproduced by a one-dimensional model of coherent field propagation in an ensemble of quantum two-level systems that self-consistently incorporates multiple scattering contribution. Our model shines light upon the key role of incoherent scattering on the modification of the optical response of dense ensembles and leads to a generalization of the Beer-Lambert law. Our result applies to any effective two-level system ensemble and allows for quantitative and absolute *in situ* absorption imaging.

I. INTRODUCTION

The formal description of light propagation in a dilute medium was first reported by Bouguer [1], and later rediscovered by Beer and Lambert [2,3]. As the Beer-Lambert law (BLL) is a single-particle model, it discards multiple scattering (MS), a mode of light transport challenging to account for, but of utmost importance in various situations, ranging from light localization [4], tumor cell detection [5] to diffuse reflectance on epithelial layers [6]. MS is also of theoretical interest as it provides a tool for testing models of long-range forces [7] and perturbative models of light transport [8].

The generalization of the BLL (gBLL) to optically dense systems requires one to use large saturation parameters of the order of the optical density [9] that generate large incoherent scattering intensities. The single-particle response is exact and very well characterized experimentally in both unsaturated and saturated regimes [10–12], and a gBLL can be derived, yielding a decay of the light intensity following the Lambert W function [13]. This solution is exact in a dilute medium of two-level systems (TLSs) and was used to develop absorption imaging techniques and derivatives [14]. The single-particle picture breaks down when increasing the density as high-order correlations between scatterers must be computed [15] and the global geometry of the medium must be carefully considered as seen experimentally with endfire superradiance [16], or as predicted theoretically in the spectroscopy of two-dimensional (2D) arrays of atoms [17]. It is widely accepted that collective phenomena in dense media scale with powers of the optical density [18,19] which is precisely the quantity that BLL endeavors to estimate.

Within the cold atom community, Reinaudi *et al.* [20] originally proposed to globally account for any deviation of the gBLL via a single heuristic reduction factor α of the bare scattering cross section σ_0, for which they proposed an experimental calibration method. α was used in experiments as a holdall that subsumes the undesired complexity arising from the presence of stray magnetic fields, imperfect probe polarization, MS, or even the multilevel structure. The reduction factor α has been estimated independently in numerous experiments [20–27] with large deviations from the ideal TLS case ($\alpha = 1$) and even very disparate results for similar probe conditions (see Table I). By solving the multilevel optical Bloch equations, α could be derived analytically [28] for a linear polarization and numerically [29] for any other polarization. In [29], it was also shown that stray magnetic fields or an imperfect probe polarization have little influence on α especially for a σ polarization, while an incoherent electromagnetic background dramatically increases its value, indicating an absolute need to account for MS.

In this paper, we show experimentally that the value of α scales linearly with the optical density which is a clear deviation from the single-particle dynamics (Sec. II). Under resonant saturated illumination, we actually expect that *incoherent* scattered fields will be reabsorbed by neighboring atoms and modify their coherent response in the forward and backward directions [30,31]. To study their influence, in Sec. III we propose a 1D model of light propagation that self-consistently includes MS at the lowest order, and recover with excellent agreement the linear dependence of α on the optical density. This result suggests that the cooperative response of dense media can be incorporated in a single-particle gBLL. The conclusion is given in Sec. IV.

II. EXPERIMENT: SCALING OF THE SCATTERING CROSS-SECTION WITH THE OPTICAL DENSITY

The derivation of the gBLL is strongly connected to the single-atom *coherent* scattering rate. For a continuous ensemble, the summation of these coherent scatterings leads to

---

*Corresponding author: simon.bernon@institutoptique.fr

TABLE I. Calibration factor α reported in the literature for thermal clouds in magneto-optical traps (MOT) or Bose-Einstein Condensates (BEC).

α	b_0	Cloud type	Probe polarization	Ref.
1.13(2)	0.5	BEC	Circular	[25]
1.11	1.2	BEC	Circular	[26]
2.0(2)	2.5	1D Li condensate	Circular	[24]
3.15(12)	5	1D BEC	Circular	[21]
2.12(1)	4.8	2D MOT	Linear	[20]
2.6(3)		Quasi-2D BEC		[22]
2.9	8.4	MOT	Linear	[23]

a differential equation of propagation of the coherent field. Reformulated as an intensity attenuation, this equation corresponds to the gBLL which is valid in any saturation regime (see Appendix A 1). The optical density is then obtained by a simple analytical integration [20]:

$$b(x, y) = -\alpha \ln [T(x, y)] + s_c[1 - T(x, y)], \quad (1)$$

where $s_c = I_0/I_{\text{sat}}$ is the saturation parameter, $T(x, y) = \frac{I(x,y)}{I_0(x,y)}$ the probe transmission, and $I_0(x, y)$ the incident imaging beam intensity. I_{sat} is the saturation intensity of a closed TLS which is related to the on-resonance cross section of a TLS $\sigma_0 = 6\pi/k^2 = \hbar\omega\Gamma/(2I_{\text{sat}})$, with $k = \omega/c$ the probe wave vector and Γ the excited state natural linewidth.

The optical density being an intrinsic cloud quantity, it should be independent of the probe beam properties. Following [20], the value of α in Eq. (1) can be determined by minimizing the influence of the intensity of the probe on the measured optical density. In the following, we show experimentally that α depends on the optical density. We then propose a model that emphasizes the role of incoherent scattering from the ensemble.

Experimentally, we prepare thermal atoms in a pure $|F_g = 1, m_F = -1\rangle$ spin state in a crossed dipole trap formed by two orthogonal 1064-nm Gaussian beams. The dipole trap depths are $U_1, U_2 = 33(3), 11(1)$ μK with, respectively, beam waists of $w_1, w_2 = 50(1), 65(1)$ μm. The cloud temperature is $T = 2.2(2)$ μK with a total atom number of $N_{\text{tot}} = 1.92(15) \times 10^5$ measured by absorption imaging of a low saturation, π-polarized probe after long time-of-flight (TOF; $b_{\text{max}} < 0.5$). The *in situ* expected widths of this thermal cloud are $\sigma_x, \sigma_y = \sqrt{k_b T/m\omega_i^2} = 6.5(5), 14.6(9)$ μm as calculated from the measured temperatures and trap angular frequencies $\omega_x, \omega_y = \sqrt{4U/m w_i^2} = 2\pi.358(18), 159(8)$ rad/s. The magnetic field at the atoms position is characterized by microwave (MW) spectroscopy and compensated for, below 10 mG. A constant offset of $B_0 = 512$ mG is then applied along the imaging beam propagation axis (i.e., gravity axis). Its direction matches a σ_- configuration of the circularly polarized imaging probe [Figs. 1(a) and 1(b)].

From $|F_g = 1, m_F = -1\rangle$, the atoms are transferred to $|F_g = 2, m_F = -2\rangle$ by an on-resonance MW pulse. The population ratio between the two states is controlled by the MW pulse duration t_{MW}. The transfer probability $P(t_{\text{MW}}) = P_{\text{tot}} \sin^2(\pi t_{\text{MW}}/T_{\text{MW}})$ has a Rabi period $T_{\text{MW}}/2 = 28$ μs and an amplitude $P_{\text{tot}} = 0.96$ [Fig. 1(c)]. The peak atomic density
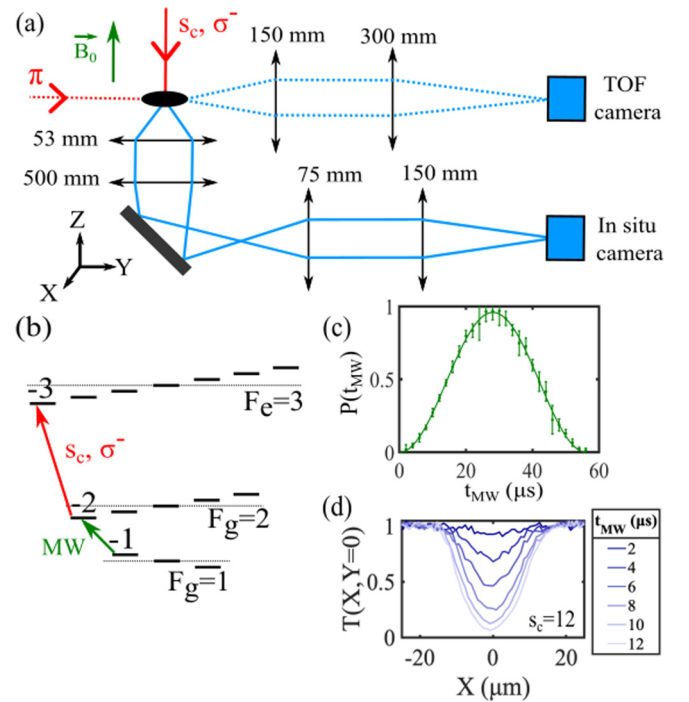

FIG. 1. (a) Experimental setup showing the two imaging axes for TOF and *in situ* absorption imaging. (b) D2-line energy structure of ^{87}Rb. (c) Rabi oscillation of the normalized atom number (points) between $|F_g = 1, m_F = -1\rangle$ and $|F_g = 2, m_F = -2\rangle$ as a function of the pulse duration and a sinusoidal fit (solid line). The data are normalized by the optically repumped total atom number. (d) Cuts along X of the transmission for $s_c = 12$.

is $n = 2.1 \times 10^{19}$ at/m^3. For $t_{\text{MW}} = 2$ μs, we expect a central optical density of 1.1(1).

Atoms in $|F_g = 2, m_F = -2\rangle$ are imaged, *in situ*, by absorption of a resonant circularly polarized imaging probe. The *in situ* imaging system consists of a microscope objective (NA = 0.44, $f_{\text{eff}} = 53$ mm) followed by a 500-mm magnification lens forming an intermediate image. A secondary telescope magnifies this image by 2 on a low noise ($<3e^-$ rms read noise) Princeton CCD camera (16 μm pixel size). For each realization, three images are acquired corresponding to the probe absorption $[I_{\text{at}}(x, y)]$, probe profile $[I_{\text{no-at}}(x, y)]$ and background $[I_{\text{at}}(x, y)]$. To minimize the influence of air turbulence, the consecutive images are taken 400 μs apart. A circular aperture with a 3 mm diameter in the Fourier plane of the secondary telescope reduces the effective NA to 0.185 and increases the depth of field to 22 μm, larger than the cloud width. The Gaussian probe profile has a waist $w = 1.13(5)$ mm. Using the intermediate imaging plane, we measured a radial positioning offset of 464 μm between the probe profile center and the cloud center leading to a reduction factor of the intensity on the atoms by 0.71 with respect to the probe center.

To quantitatively explore various optical density regimes only the MW duration ($t_{\text{MW}} = [2, 4, 6, 8, 10, 12]$ μs) is changed. For the scanned probe saturation parameters ($s_c = [0.44, 0.63, 1.36, 2.2, 4.9, 7.8, 12.3, 16.3, 20.9, 28, 37.3, 49]$), the probe pulse duration is adjusted from 12.9 to 3.7 μs to
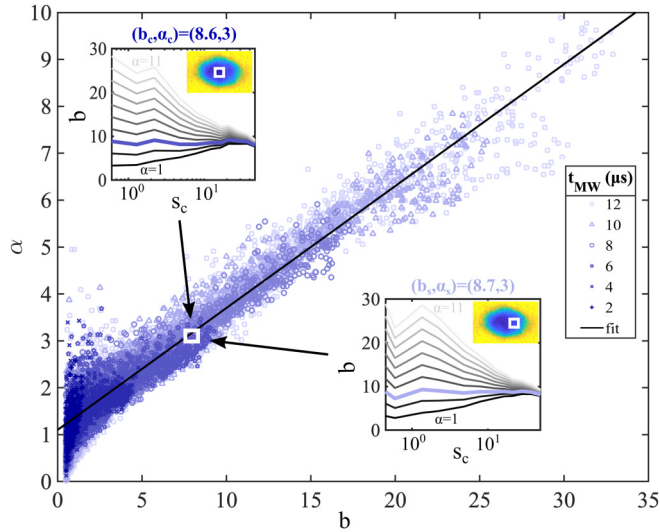
FIG. 2. Correction factor α vs the optical density for all MW datasets (2, 4, 6, 8, 10, 12 μs). Each point corresponds to 1 pixel and the solid line is a linear fit to the data $\alpha = 1.17(9) + 0.255(2)b$.

maintain the number of scattered photons per atom at around 70. In absence of atoms and taking into account the imaging system transmission ($T_{\rm im} = 0.76$), each pixel receives in between 200 and 6500 photons depending on the probe saturation parameter. Each couple of parameters [$t_{\rm MW}, s_c$] is repeated five times for averaging. Shot-to-shot fluctuations of the saturation intensity are compensated by acquiring each imaging pulse by a calibrated photodiode.

Following the spirit of [20], for each MW duration we use the local transmission $T(x, y) = (I_{\rm at} - I_{\rm back})/(I_{\rm no\text{-}at} - I_{\rm back})$ acquired for the various saturation intensity and compute, for every pixel (x, y), the couple of parameters $\{b(x, y), \alpha(x, y)\}$ that makes b [Eq. (1)] independent of the probe saturation. The resulting parameters are plotted in Fig. 2 where a clear correlation can be observed.

In the insets, we show ten curves of b vs s_c corresponding to α varying from 1 (black) to 11 (light gray). The best value of α minimizes $std(b)$. To reject the noise at very low transmission that is influenced by camera read noise and fluorescence, that might cause systematic errors, we limit the analysis to transmissions T in the range [0.05, $+\infty$[. From the value of α, the optical density is obtained by averaging it over all values of s_c. The upper inset corresponds to a pixel at the center of the cloud with $t_{\rm MW} = 6$ μs : $(b_c, \alpha_c) = (8.6, 3)$ and the lower inset to a side shifted pixel for $t_{\rm MW} = 10$ μs : $(b_s, \alpha_s) = (8.7, 3)$. The position offset of these two pixels compensates for the difference of central densities of their respective clouds, giving rise to a similar local optical density. Independently from their difference of position in the cloud, equivalent local optical densities lead to the same reduction of the scattering cross section. A linear fit of the entire dataset in Fig. 2 gives a slope of 0.255(2) and an offset of 1.17(9) where the uncertainty is dominated by the uncertainty of the saturation parameter. This offset close to 1 shows that in the limit of low densities the atomic response is well modeled by an ensemble of independent TLSs. The value of α at low atomic density depends on both the probe polarization and the

magnetic field direction but also linearly depends on the calibration of the saturation intensity as observed by the atomic cloud. The calibration of the offset between probe center and atoms was important in this respect. The dependence of α on b shows that α is not solely determined by the probe properties but also depends on the optical density which is a signature of the influence of MS.

III. MODEL: LIGHT PROPAGATION IN 1D WITH INCOHERENT MULTIPLE SCATTERING

To account for MS, we propose a model of saturated propagation that can be quantitatively compared to the data. Under a saturating coherent probe, a single atom emits coherent and incoherent light, the latter physically corresponding to the Mollow's spectrum. Our model derives the propagation of each component and accounts for their nonlinear coupling through atomic saturation. The system we consider is a coherent probe propagating along z in a cloud that is homogeneous in the transverse directions and has a Gaussian density profile along z. As the system is translation invariant in the transverse plane (x, y), there can be no net transverse energy flux and scatterings only redistribute in the forward and backward directions. Therefore, we use a 1D model where the electromagnetic field and intensity only depend on z. For a resonant σ-polarized probe, the scattering properties of an atom embedded in an incoherent electromagnetic background are well described [29] by an effective TLS. To numerically solve our model, we divide the propagation direction in infinitely small slabs of width dz (see Appendix A 2). For each slab, we derive a set of differential equations that relates the intensity profile of the coherent intensity $I_c(z)$, forward incoherent intensity $I_i^+(z)$, and backward incoherent intensity $I_i^-(z)$. The set of equations is expressed in terms of the nondimensionalized saturation intensity parameters $s_c(z) = I_c(z)/I_{\rm sat}$, $s_i^+(z) = I_i^+(z)/I_{\rm sat}^{\rm iso}$, and $s_i^-(z) = I_i^-(z)/I_{\rm sat}^{\rm iso}$ where $I_{\rm sat}^{\rm iso} = \alpha^{\rm iso} I_{\rm sat} = 2.12 I_{\rm sat}$:

$$\frac{ds_c}{dz} = -n(z)\sigma_0 \frac{s_c}{1 + s_c + s_i},$$

$$\frac{ds_i^{(\pm)}}{dz} = -\frac{n(z)\sigma_0^{\rm iso}}{2} \left(\frac{s_i^{(\pm)} - s_i^{(\mp)}}{1 + s_c + s_i} \right.$$
$$\left. - \frac{s_c(s_c + s_i)}{(1 + s_c + s_i)^2} - \frac{s_c}{(1 + s_c + s_i)^2} \right), \quad (2)$$

where the isotropic cross section is $\sigma_0^{\rm iso} = \hbar\omega\Gamma/(2I_{\rm sat}^{\rm iso})$ and the total incoherent intensity is $s_i = s_i^{(+)} + s_i^{(-)}$. Although incoherent fields have off-resonance spectral components [32], we consider their rescattering to behave as an on-resonance spectrum with a reduced isotropic scattering cross section [30,31]. The prefactor $1/2$ accounts for equally distributed backward and forward scattered intensities. In the derivatives of $s_i^{(\pm)}$ in Eqs. (2), the first term accounts for rescattering of the incoherent field, and the second one accounts for the temporally incoherent scattering of the coherent field (i.e., *resonant fluorescence*). The last term that conserves energy corresponds to the coherent field scattering in a temporally coherent but spatially incoherent field arising from the discrete random position of atoms in
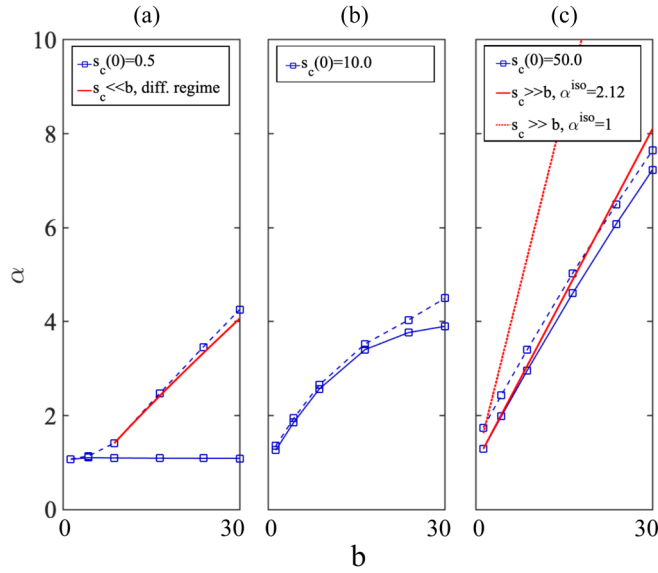
FIG. 3. α parameters calculated from the 1D saturated scattering model [Eq. (2)]. The simulated probe saturation intensities are comparable to the experiment: (a) $s_c = 0.5$, (b) $s_c = 10$, and (c) $s_c = 50$. The blue line (respectively, blue dashed line) corresponds to the value of α as calculated from the sole coherent transmission $T_c = s_c(L)/s_c(0)$ [respectively, the total transmission $T = [s_c(L) + \alpha^{\mathrm{iso}} s_i^+(L)\Omega/(2\pi)]/s_c(0)$, where $\alpha^{\mathrm{iso}} s_i^+(L)\Omega$ is the fluorescence background emitted in the solid angle Ω of the imaging system]. In red in (a) is the limit of diffusive regime (see text); and in (c) the analytical large saturation limit for (plain line) an effective TLS approximation of a MLS with $\sigma_0^{\mathrm{iso}} = \sigma_0/\alpha^{\mathrm{iso}}$, and (dotted line) an ideal scalar TLS corresponding to $\sigma_0^{\mathrm{iso}} = \sigma_0$.

an ensemble. This spatially incoherent field is out of phase with the coherent probe and its effect on the coherence term of the density matrix ρ_{eg} will spatially average to 0. As checked numerically, for large saturation, the scattering being mostly temporally incoherent, the directionality of spatially incoherent scattering (forward, backward, or equally distributed) has no influence on the value of α. In this model, both temporally and spatially incoherent contributions are summed in the incoherent intensities $(I_i^{(\pm)})$. Summing incoherent intensities is justified by the independent scattering approximation [8], valid for $(kl_{\mathrm{sc}})^{-1} \ll 1$, with $l_{\mathrm{sc}} = 1/(n\sigma_0)$ the photon mean free path. Our largest optical density of 30 gives $(kl_{\mathrm{sc}})^{-1} = 0.25$.

From the solution of Eqs. (2), the value of α is obtained for different probe intensities and presented in Fig. 3 as a function of the integrated optical density.

For small probe saturation [Fig. 3(a)], the conversion of the coherent probe field into incoherent intensity (s_i) cannot generate high incoherent intensity ($s_i \ll 1$) and should therefore not affect the value of α in the coherent propagation [Eqs. (2)]. Nevertheless, for high optical density, we are in the diffusive regime. Along the propagation, while the coherent field is exponentially reduced in the mean free path length l_{sc} and quickly disappears, the incoherent field, that will also be detected on the camera, is only algebraically reduced, $T_{\mathrm{diff}} \propto 1/b = C/b$ [33,34]. In this regime ($b \gg s_c$), $\alpha \approx b/\ln[2\pi b/(C\Omega)]$ is dominated by the diffuse transmis-

sion [dashed red asymptote in Fig. 3(a) with $C = 1$] where Ω is the solid angle of the imaging system. This lower limit of α does not correspond to a reduction of the absorption cross section but rather to an excess of detected light and is mostly constant over a wide range of solid angles (see Appendix A 2).

In the opposite high saturation regime $s_c \gg b$ [Fig. 3(c)], the probe intensity is little depleted, and the incoherent saturation intensity becomes homogeneous along the propagation. By energy conservation we have $s_i = s_c(1 - T)/(2\alpha^{\mathrm{iso}})$. For high saturation, the last term in Eq. (1) dominates in the expression of the optical density: $b \approx s_c(1 - T)$. It leads to a reduction of the coherent absorption cross section that scales as $\alpha = 1 + s_i \approx 1 + b/(2\alpha^{\mathrm{iso}})$ [red curve in Fig. 3(c)]. The intermediate regime of saturation [Fig. 3(b)] lies in-between the two theoretical limits. The equivalence between s_i and b at large s_c unravels the nonlocal character of the incoherent saturation intensity. This upper limit of the slope is evaluated for two models of incoherent scattering interaction considered either σ polarized ($\alpha^{\mathrm{iso}} = 1$) or isotropic ($\alpha^{\mathrm{iso}} = 2.12$), giving, respectively, a slope of $1/2$ and $1/(2 \times 2.12) = 0.24$. The experimental data lie in-between the above-mentioned lower and upper theoretical limits indicating that, even if the 1D model neglects to account for the cloud inhomogeneity, it still captures the MS origin of the increase of α with b.

IV. CONCLUSION

In contrast with the commonly used calibration methods of the reduction factor α of the scattering cross section [20], this study shows that α is not unique for an inhomogeneous ensemble. Via a 1D model, we have shown that the reduction of the apparent absorption cross section is connected, in the diffusive regime ($b \gg s_c$), to the residual diffuse transmission and, in the saturating regime, to the ambient electromagnetic background originating from multiple incoherent scattering in the cloud. In both cases, this reduction is shown to scale mainly linearly with the local optical density. For a circular probe polarization under a well-controlled magnetic field orientation and laser detuning, the slope of the correction factor, $\alpha = 1.17(9) + 0.255(2)b$, is independent of the transverse position in the cloud. Our model suggests that this slope is applicable to any ensemble of effective TLS. The offset $\alpha_0 = 1.17(9)$ ultimately depends on a fine calibration of the saturation parameter and should be 1 for a perfect σ light. Using Eq. (1) and $d\alpha/db = 0.255(2)$, we obtain a gBLL expression of the optical density that accounts for MS:

$$b(x, y) = \frac{-\alpha_0 \ln[T(x, y)] + s_c[1 - T(x, y)]}{1 + \frac{d\alpha}{db} \ln[T(x, y)]}. \quad (3)$$

A similar calibration could certainly be performed for other probe configurations such as linear π probes. A strength of the proposed model is to take into account both the saturated response of a single atom embedded in an electromagnetic environment and the collective participation of the surrounding atoms to this environment in a self-consistent solution. At the cost of numerical computation power, the proposed 1D model could certainly be extended to three dimensions to account for the transverse inhomogeneity of the ensemble and

further incorporate multilevel internal dynamics influence on the reabsorption cross section.

Note added. Recently, we become aware of a related work from Jan Arlt's group [35].

APPENDIX

This Appendix contains two sections. In Sec. 1 we derive, under the continuous medium approximation, the Beer-Lambert's law in any saturation regime for an ensemble of effective two-level systems. In Sec. 2, we detail the derivation of the set of coupled equations [Eqs. (2)] in the main text and the numerical resolution method.

1. Beer-Lambert derivation in the saturating regime

In this section, we will derive the differential equation of propagation of a probe radiation (considered as a coherent field) in a continuous medium. The field at the point r is obtained by summing the coherent incident field $\boldsymbol{E}(\boldsymbol{r}) = \frac{E_A}{2}e^{ikz}\boldsymbol{\epsilon}$ with polarization $\boldsymbol{\epsilon}$ and the total scattered field $\boldsymbol{E}_{\text{tot}}(\boldsymbol{r'})$:

$$\boldsymbol{E}(\boldsymbol{r'}) = \boldsymbol{E}(\boldsymbol{r}) + \boldsymbol{E}_{\text{tot}}(\boldsymbol{r'}). \tag{A1}$$

The total scattered field in Eq. (A1) is obtained by integrating over space the fields emitted by a continuous ensemble of dipoles [11,36]:

$$\boldsymbol{E}_{\text{tot}}(\boldsymbol{r'}) = \iiint_V n(\boldsymbol{r})E_{\text{sca}}(\boldsymbol{r},\boldsymbol{r'})[\boldsymbol{\epsilon} - (\boldsymbol{\epsilon}.\boldsymbol{u}_{rr'})\boldsymbol{u}_{rr'}]d\boldsymbol{r}^3, \tag{A2}$$

where $E_{\text{sca}}(\boldsymbol{r},\boldsymbol{r'}) = \frac{3E_A}{2k}e^{ikz}i\frac{e^{ik|\boldsymbol{r'}-\boldsymbol{r}|}}{|\boldsymbol{r'}-\boldsymbol{r}|}$ is the scattered field amplitude, $\boldsymbol{u}_{rr'} = (\boldsymbol{r'}-\boldsymbol{r})/|\boldsymbol{r'}-\boldsymbol{r}|$ is a vector unit, $n(\boldsymbol{r})$ is the atomic density, and V is the volume of integration. For an infinite homogeneous slab of atoms of width dz, the integration is carried for x, y in $]-\infty, +\infty[$ and z in $[z, z+dz]$.

In Eq. (A2), we consider only the dipole scattering in the far-field regime varying in $1/r$ which corresponds well to the regime of the data presented in the main text ($nk^{-3} \ll 1$). We also emphasize that the above expression is only valid in the weak saturation approximation when a TLS is well approximated by a dipole. Performing the integration in cylindrical coordinates over a circle $R_0 \gg 1/k$ (i.e., ignoring edge effects) for a constant atomic density in this disk $n(\boldsymbol{r}) = n(z)$ and a circular polarization $\boldsymbol{\epsilon}_+$, the first term proportional to $\boldsymbol{\epsilon}$ which is the on-axis scattering becomes $-n(z)\frac{3E_A}{2k^2}e^{ik(z+dz)}2\pi\boldsymbol{\epsilon}_+ dz$ and the second term depending on $\boldsymbol{u}_{rr'}$, which is the off-axis scattering, reads $n(z)\frac{3E_A}{2k^2}e^{ik(z+dz)}\pi\boldsymbol{\epsilon}_+ dz$. Equation (A2) can then be simplified

into

$$\boldsymbol{E}(z+dz) = \boldsymbol{E}(z)\left(1 - \frac{n(z)}{2}\frac{6\pi}{k^2}e^{ikdz}dz\right), \tag{A3}$$

which can be reformulated in a differential expression of the Beer-Lambert's law in field:

$$\frac{d\boldsymbol{E}}{dz} = -\boldsymbol{E}\frac{n(z)\sigma_0}{2}e^{ikdz}, \tag{A4}$$

where $\sigma_0 = 6\pi/k^2$ is the on-resonance absorption cross section. For $kdz \ll 1$, Eq. (A4) gives the standard exponential attenuation of the intensity:

$$\frac{d|\boldsymbol{E}|^2}{dz} = -|\boldsymbol{E}|^2 n(z)\sigma_0. \tag{A5}$$

When the medium is saturated, the amplitude of the coherent field emitted on resonance by a single TLS is reduced but its radiation pattern for a given driving field polarization is unchanged. The volume integral carried in Eq. (A2) is still exact but the integral is globally reduced by a factor $1/(1 + s_c)$ where $s_c = 2\Omega_c^2/\Gamma^2$ is the saturation parameter and Ω_c the Rabi frequency proportional to the incident electric field amplitude. This reduction factor of the coherently emitted field is directly related to the coherent scattering rate $\Gamma|\rho_{eg}|^2 = \frac{\Gamma}{2}\frac{s_c}{(1+s_c)^2}$ that can be derived from the optical-Bloch equations of a TLS. To take into account the effect of saturation, the equation of propagation in field [Eq. (A3)] is modified into

$$\boldsymbol{E}(z+dz) = \boldsymbol{E}(z)\left(1 - \frac{1}{(1+s_c)}\frac{n(z)}{2}\frac{6\pi}{k^2}e^{ikdz}dz\right), \tag{A6}$$

which gives the general form of the Beer-Lambert's law in intensity I for any saturation regime:

$$\frac{dI(z)}{dz}\left(1 + \frac{I(z)}{I_{\text{sat}}}\right) = -n(z)\sigma_0 I(z), \tag{A7}$$

where I_{sat} is the saturation intensity which is related to the cross section by $\sigma_0 = \hbar\omega\Gamma/(2I_{\text{sat}})$. For a multilevel system, it can be shown [29] that the coherent scattering rate is reduced and takes the form $\Gamma|\rho_{eg}|^2 = \frac{\Gamma}{2}\frac{s_c}{(\alpha+s_c)^2}$ where α depends on the probe polarization, residual magnetic field, detuning from the resonance or the ambient electromagnetic background. In other words, it reduces (respectively, increases) the cross section (respectively, the saturation intensity) by a factor α. For ^{87}Rb, on resonance with the $|5S_{1/2}, F_g = 2\rangle$ to $|5P_{3/2}, F_e = 3\rangle$ cycling transition, a resonant probe with circular polarization has $\alpha = 1$ (i.e., a perfect two-level system), $\alpha = 1.829$ for linear polarization, and $\alpha \in [1, 1.829]$ for any other probe polarization. Including this correction in the above derivation, Eq. (A7) becomes

$$\frac{dI}{dz}\left(\alpha + \frac{I}{I_{\text{sat}}}\right) = -n(z)\sigma_0 I. \tag{A8}$$

Using the saturation intensity for the coherent field $s_c(z) = I(z)/I_{\text{sat}}$, Eq. (A8) can be written as

$$\frac{ds_c}{dz} = -n(z)\sigma_0\frac{s_c(z)}{\alpha + s_c(z)}, \tag{A9}$$

which gives the first equation of the 1D propagation model in the main text with $\alpha = 1 + s_i$. We stress that this equation has been obtained via the coherent propagation of the probe field.
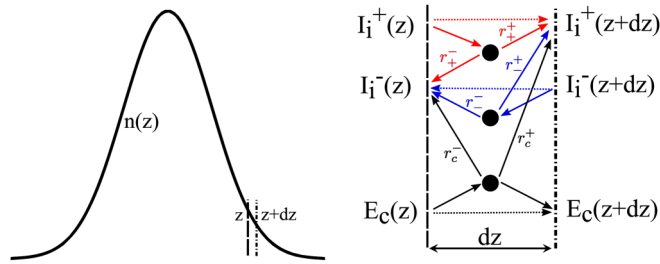
FIG. 4. 1D model for the coherent and incoherent propagation and conversion of light between adjacent layers. The coherent and incoherent scattering rates are given by Eq. (A10). The spatial repartition is taken as $r_+^+ = 1 - r_+^- = r_-^- = 1 - r_-^+ = r_c^+ = 1 - r_c^- = 1/2$ (see text).

Equation (A9) can be analytically integrated over the propagation direction which leads to the expression of the optical density in the saturating regime given by Eq. (1) in the main text.

2. 1D propagation model

a. Derivation of the set of coupled equations

In this section, we detail the derivation of Eqs. (2) in the main text which arise from a self-consistent influence of the

coherent field on the incoherent intensity propagation and vice versa. The coherent and total scattering rates of a two-level system, as deduced from the density matrix calculations, are given by [29]

$$R_{\text{sca}}^{(\text{coh})} = \frac{\Gamma}{2\alpha} \frac{s_c/\alpha}{(1 + s_c/\alpha)^2},$$

$$R_{\text{sca}}^{(\text{tot})} = \frac{\Gamma}{2} \left(\frac{s_c/\alpha}{1 + s_c/\alpha} + \frac{s_i/\alpha_c}{1 + s_i/\alpha_c} \right), \quad \text{(A10)}$$

where the corrected scattering rates are $\alpha = \alpha_{\text{SA}}(1 + s_i)$ and $\alpha_c = 1 + s_c$, where α_{SA} is the single-atom reduction of the cross section that depends on polarization, detuning, and magnetic field offset. In this work, we have $\alpha_{\text{SA}} = 1$ corresponding to on-resonance σ polarization. The single-atom incoherent rate $R_{\text{sca}}^{(\text{inc})} = R_{\text{sca}}^{(\text{tot})} - R_{\text{sca}}^{(\text{coh})}$ can be written as

$$R_{\text{sca}}^{(\text{inc})} = \frac{\Gamma}{2} \left(\frac{s_i}{1 + s_c + s_i} + \frac{s_c(s_c + s_i)}{(1 + s_c + s_i)^2} \right). \quad \text{(A11)}$$

This incoherent scattering rate is responsible for a re-homogenization of the forward and backward incoherent intensities in a layer dz and corresponds to the first and second terms in the 1D differential equations of incoherent intensity ($s_i^{(\pm)}$) propagation [Eqs. (2) in the main text]. In Fig. 4,
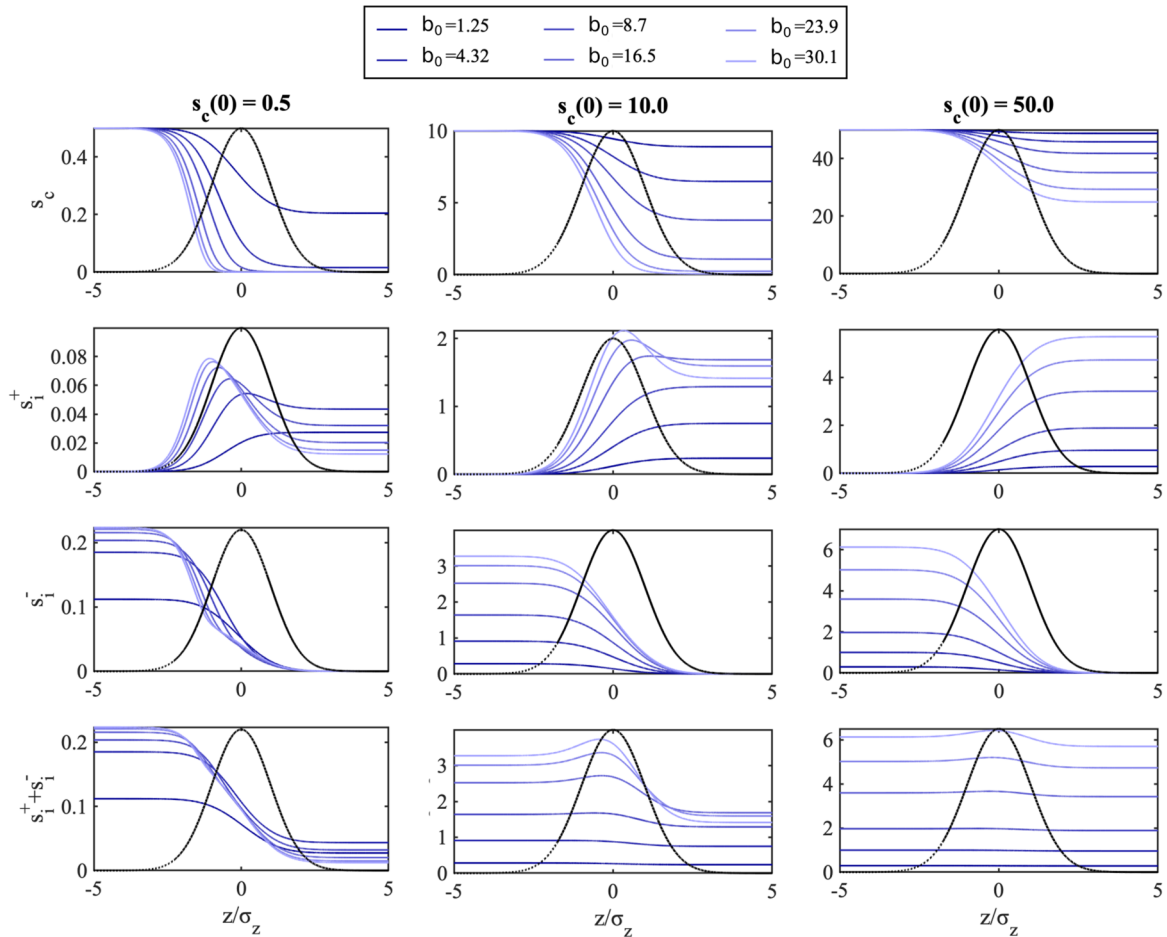

FIG. 5. Saturation profiles of for the coherent part $s_c(z)$ and incoherent parts $s_i^+(z)$, $s_i^-(z)$, and $s_i^+(z) + s_i^-(z)$ for coherent input saturations of $s_c(0) = 0.5, 10, 50$ and optical densities b_0 from 1.25 (dark-blue solid line) to 30.1 (light-blue solid line). The black dotted line is the Gaussian atomic density profile with an arbitrary amplitude to match the plot size. The x axis is normalized by the Gaussian width $\sigma_z = 5 \ \mu$m.

$r_+^+ = r_-^- = 1/2$ and $r_-^- = r_+^+ = 1/2$ account for an isotropic rescattering of the incoherent field; $r_c^{-,ti} = r_c^{+,ti} = 1/2$ is well justified by the fact that temporally incoherent (ti) scattering of the incident coherent field cannot interfere and therefore has no preferred direction. It follows the radiation pattern of the probe polarization giving rise to an equal amount of backward and forward incoherent scattering. $r_c^{-,si} = r_c^{+,si} = 1/2$ account for the incident coherent probe being scattered in a spatially incoherent (si) field. It leads to the last term in Eqs. (2) which guarantees the conservation of energy. The temporally and spatially incoherent contributions are summed in the incoherent intensity: $r_c^{+/-} = r_c^{+/-,ti} + r_c^{+/-,si}$.

b. Iterative numerical solution

The solution for the set of coupled equations [Eqs. (2)] are obtained by an iterative process similar to a perturbation approach. We note (i) the ith step of the iteration. At step 0, the spatial profile of the coherent intensity $[s_c^{(0)}(z)]$ is determined without considering the influence of the incoherent background $(s_i^{+/-,(0)} = 0)$. Then at step $(i + 1)$, the equation for $s_i^{+,(i+1)}(z)$ is numerically integrated with $s_c = s_c^{(i)}(z)$, $s_i^- = s_i^{-,(i)}$, and the boundary condition $s_i^{+,(i+1)}(-\infty) = 0$. A similar calculation is carried for $s_i^{-,(i+1)}(z)$ with $s_c = s_c^{(i)}(z)$, $s_i^+ = s_i^{+,(i)}(z)$, $s_i^{-,(i+1)}(\infty) = 0$, and for $s_c^{(i+1)}(z)$ with $s_i^- = s_i^{-,(i+1)}(z)$, $s_i^+ = s_i^{+,(i+1)}(z)$, and $s_c^{(i+1)}(-\infty) = s_c^0$. In other words, we iteratively reinject the solution of step (i) into the equation for step $(i + 1)$ and converge towards an autoconsistent solution that no longer varies in between successive steps. At this stage, our set of equations is considered as solved for the particular input coherent intensity $(s_c^{(0)})$ and atomic density $[n(z)]$.

c. Steady-state solutions

Figure 5 shows the steady-state intensity profiles along the propagation direction obtained for various saturation s_c and optical density b. At a low saturation $[s_c(0) = 0.5]$, as b increases, the coherent field gets converted into incoherent light at the entrance of the cloud. Most of the incoherent intensity is converted into s_i^- as the probability for a photon to pass through the cloud gets reduced. As $s_c(0)$ increases, more coherent intensity passes through the cloud. The cross section is then mostly determined by the coherent saturation parameter. At large saturation $[s_c(0) = 50]$, the incoherent intensity is homogeneous along the propagation direction as most of the coherent light is transmitted.

From these profiles, the expected α can be calculated using the transmitted intensities. The reduction of the cross section α is computed numerically from the coherent transmission $[s_c(\infty)]$ and the incoherent intensity $[s_i^+(\infty)]$ collected in a solid angle Ω and inverting the equation giving the optical density [Eq. (1)]:

$$\alpha = \frac{-b - [s_c(\infty) + s_i^+(\infty)\Omega\alpha_{iso} - s_c(0)]}{\ln\{[s_c(\infty) + s_i^+(\infty)\Omega\alpha_{iso}]/s_c(0)\}}. \quad (A12)$$

As final remarks, we focus on the transmitted incoherent intensity $\frac{s_i^+(\infty)}{s_c(0)}$ and the influence of the solid angle. Figure 6 gives this incoherent transmission as a function of the optical density for three initial values of $s_c(0)$. At fixed $s_c(0)$, the
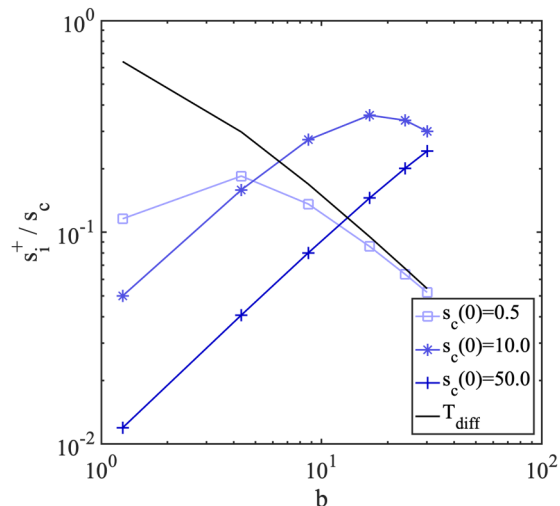

FIG. 6. Forward incoherent transmission vs the optical density for three initial coherent saturations (blue lines). The black line is the diffuse transmission given by T_{diff}.

initial increase of the incoherent transmission as a function of the optical density means that the coherent intensity is initially converted by incoherent scattering into an incoherent propagating intensity. On the other hand, in the large optical density limit $(b \gg s_c)$, the residual diffuse transmission obtained with our model tends towards the analytical limit $T_{diff} = \frac{1 + 0.7104}{b + 2 \times 0.7104}$ [34] which was obtained from a model of light propagation in an homogeneous slab that excludes coherence and interference effects (diffuse equation or random walk).

Finally, we evaluate the impact of the solid angle where a part of the incoherent intensity (incoherent transmission) is measured by the camera. Figure 7 shows α as a function of $\Omega/(2\pi) \in [0, 0.017]$ for a large optical density of 30.1. The upper value of Ω corresponds to the experimental case (NA = 0.185) in the main text. We see that for $s_c(0) \gg 1$, the value of α is approximately constant over a wide range of solid angles. The effect is a bit more
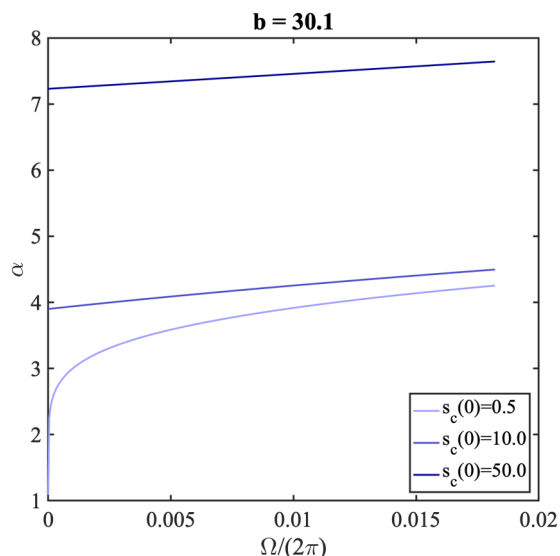

FIG. 7. Influence of the solid angle on the value of α at a large optical density and for three initial saturations.

important for $s_c(0) < 1$ where the sensitivity for low transmissions is sharp, due to the logarithm term in the optical density.

However, it remains constant in a wide range of solid angles $[\Omega/(2\pi) > 10^{-3}]$.

[1] P. Bouguer, *Essai d'optique, sur la gradation de la lumière* (Claude Jombert, Paris, 1729).

[2] J. H. Beer, Bestimmung der absorption des rothen lichts in farbigen Flüssigkeiten, Ann. Phys. (Berlin) **162**, 78 (1852).

[3] J. H. Lambert, Photometria Sive de Mensura et Gradibus Luminis, Colorum et Umbrae (Augustae Vindelicorum, Klett, 1760).

[4] N. Cherroret, M. Hemmerling, G. Labeyrie, D. Delande, J. T. M. Walraven, and R. Kaiser, Weak localization of light in hot atomic vapors, Phys. Rev. A **104**, 053714 (2021).

[5] L. T. Perelman, V. Backman, M. Wallace, G. Zonios, R. Manoharan, A. Nusrat, S. Shields, M. Seiler, C. Lima, T. Hamano, I. Itzkan, J. Van Dam, J. M. Crawford, and M. S. Feld, Observation of Periodic Fine Structure in Reflectance from Biological Tissue: A New Technique for Measuring Nuclear Size Distribution, Phys. Rev. Lett. **80**, 627 (1998).

[6] G. Zonios and A. Dimou, Modeling diffuse reflectance from homogeneous semi-infinite turbid media for biological tissue applications: A Monte Carlo study, Biomed. Opt. Express **2**, 3284 (2011).

[7] L. G. F. Soares and F. Haas, Nonlinear oscillations of ultra-cold atomic clouds in a magneto-optical trap, Phys. Scr. **94**, 125214 (2019).

[8] C. C. Kwong, D. Wilkowski, D. Delande, and R. Pierrat, Coherent light propagation through cold atomic clouds beyond the independent scattering approximation, Phys. Rev. A **99**, 043806 (2019).

[9] A. Reinhard, J.-F. Riou, L. A. Zundel, and D. S. Weiss, Dark-ground imaging of high optical thickness atom clouds, Opt. Commun. **324**, 30 (2014).

[10] G. Wrigge, I. Gerhardt, J. Hwang, G. Zumofen, and V. Sandoghdar, Efficient coupling of photons to a single molecule and the observation of its resonance fluorescence, Nat. Phys. **4**, 60 (2008).

[11] M. K. Tey, G. Maslennikov, T. C. H. Liew, S. A. Aljunid, F. Huber, B. Chng, Z. Chen, V. Scarani, and C. Kurtsiefer, Interfacing light and single atoms with a lens, New J. Phys. **11**, 043011 (2009).

[12] E. W. Streed, A. Jechow, B. G. Norton, and D. Kielpinski, Absorption imaging of a single atom, Nat. Commun. **3**, 933 (2012).

[13] H. Abitan, H. Bohr, and P. Buchhave, Correction to the Beer-Lambert-Bouguer law for optical absorption, Appl. Opt. **47**, 5354 (2008).

[14] M. Pappa, P. C. Condylis, G. O. Konstantinidis, V. Bolpasi, A. Lazoudis, O. Morizot, D. Sahagun, M. Baker, and W. von Klitzing, Ultra-sensitive atom imaging for matter-wave optics, New J. Phys. **13**, 115012 (2011).

[15] M. D. Lee, S. D. Jenkins, and J. Ruostekoski, Stochastic methods for light propagation and recurrent scattering in saturated and nonsaturated atomic ensembles, Phys. Rev. A **93**, 063803 (2016).

[16] S. Inouye, A. P. Chikkatur, D. M. Stamper-Kurn, J. Stenger, D. E. Pritchard, and W. Ketterle, Superradiant Rayleigh scattering from a Bose-Einstein condensate, Science **285**, 571 (1999).

[17] R. J. Bettles, M. D. Lee, S. A. Gardiner, and J. Ruostekoski, Quantum and nonlinear effects in light transmitted through planar atomic arrays, Commun Phys **3**, 141 (2020).

[18] G. Labeyrie, D. Delande, C.A. Müller, C. Miniatura, and R. Kaiser, Coherent backscattering of light by an inhomogeneous cloud of cold atoms, Opt. Commun. **243**, 157 (2004).

[19] P. Weiss, M. O. Araújo, R. Kaiser, and W. Guerin, Subradiance and radiation trapping in cold atoms, New J. Phys. **20**, 063024 (2018).

[20] G. Reinaudi, T. Lahaye, Z. Wang, and D. Guéry-Odelin, Strong saturation absorption imaging of dense clouds of ultracold atoms, Opt. Lett. **32**, 3143 (2007).

[21] C. Mordini, D. Trypogeorgos, A. Farolfi, L. Wolswijk, S. Stringari, G. Lamporesi, and G. Ferrari, Measurement of the Canonical Equation of State of a Weakly Interacting 3D Bose Gas, Phys. Rev. Lett. **125**, 150404 (2020).

[22] T. Yefsah, R. Desbuquois, L. Chomaz, K. J. Günter, and J. Dalibard, Exploring the Thermodynamics of a Two-Dimensional Bose Gas, Phys. Rev. Lett. **107**, 130401 (2011).

[23] G. Reinaudi, Manipulation et refroidissement par évaporation forcée d'ensembles atomiques ultra-froids pour la production d'un jet intense dans le régime de dégénérescence quantique: vers l'obtention d'un laser à atomes continu, Ph.D. thesis, Université Pierre et Marie Curie-Paris VI, 2008.

[24] M. Horikoshi, A. Ito, T. Ikemachi, Y. Aratake, M. Kuwata-Gonokami, and M. Koashi, Appropriate probe condition for absorption imaging of ultracold ^{6}Li atoms, J. Phys. Soc. Jpn. **86**, 104301 (2017).

[25] E. M. Seroka, A. V. Curiel, D. Trypogeorgos, N. Lundblad, and I. B. Spielman, Repeated measurements with minimally destructive partial-transfer absorption imaging, Opt. Express **27**, 36611 (2019).

[26] M. F. Riedel, P. Böhi, Y. Li, T. W. Hänsch, A. Sinatra, and P. Treutlein, Atom-chip-based generation of entanglement for quantum metrology, Nature (London) **464**, 1170 (2010).

[27] W. J. Kwon, J.-Y. Choi, and Y.-I. Shin, Calibration of saturation absorption imaging of ultracold atom clouds, J. Korean Phys. Soc. **61**, 1970 (2012).

[28] B. Gao, Effects of Zeeman degeneracy on the steady-state properties of an atom interacting with a near-resonant laser field: Analytic results, Phys. Rev. A **48**, 2443 (1993).

[29] R. Veyron, V. Mancois, J. B. Gerent, G. Baclet, P. Bouyer, and S. Bernon, Effective two-level approximation of a multilevel system driven by coherent and incoherent fields, Phys. Rev. A **105**, 043105 (2022).

[30] L. Pucci, A. Roy, T. S. do Espirito Santo, R. Kaiser, M. Kastner, and R. Bachelard, Quantum effects in the cooperative scattering of light by atomic clouds, Phys. Rev. A **95**, 053625 (2017).

[31] This is obviously expected in the weak-saturation limit where the scattering is mainly coherent. In the strong-field limit, the scattering is mostly incoherent with a Mollow triplet spectrum [32]. Counterintuitively, the off-resonance sidebands are actually resonant with transitions of neighboring atoms. Indeed, in a dressed state picture, both the on-resonance and side-

bands correspond to emission associated to the decay between light-induced dressed states which also correspond to the absorption lines of the similarly driven neighboring atoms.

[32] B. R. Mollow, Power spectrum of light scattered by two-level systems, Phys. Rev. **188**, 1969 (1969).

[33] N. Garcia, A. Z. Genack, and A. A. Lisyansky, Measurement of the transport mean free path of diffusing photons, Phys. Rev. B **46**, 14475 (1992).

[34] W. Guerin, M. T. Rouabah, and R. Kaiser, Light interacting with atomic ensembles: Collective, cooperative and mesoscopic effects, J. Mod. Opt. **64**, 895 (2017).

[35] J. Arlt's group (private communication).

[36] L. Chomaz, L. Corman, T. Yefsah, R. Desbuquois, and J. Dalibard, Absorption imaging of a quasi-two-dimensional gas: A multiple scattering analysis, New J. Phys. **14**, 055001 (2012).